Title

Predictability of charmonium levels from a range of good fits

Permalink

https://escholarship.org/uc/item/23t9w465

Journal

Physical Review D, 48(5)

ISSN

2470-0010

Authors

Silverman, Dennis

Altshuler, Eric

Publication Date

1993-09-01

DOI

10.1103/physrevd.48.2160

Copyright Information

Peer reviewed

Predictability of charmonium levels from a range of good fits

Dennis Silverman and Eric Altshuler

Department of Physics, University of California, Irvine, Irvine, California 92717

(Received 12 February 1993)

A QCD-motivated potential with five parameters and a cutoff on high virtual momentum is used in a relativistic bound-state equation to examine the predictive power of valence quark potential models by computing fits to the seven well-established charmonium levels. The predictions of potential models are really ranges for new levels given by the ranges of parameters that give good fits to established levels, rather than the single best fit. The range of parameters that give good fits is presented in three-dimensional plots by isosurfaces of fits with fixed theoretical standard deviations in energy from the known levels. Next, for each value of a predicted splitting we show the minimum deviation found over all the fits that lead to that value of splitting. We also show correlations between predictions by finding for each pair of values for two predictions the minimum deviation among the fits that give those predicted values, and making contour plots. For the $^1P_1$-$^3P_{\text{c.g.}}$ splitting we find the predictions to cover a range of several MeV both positive and negative. A correlation of the spin-spin $^1P_1$-$^3P_{\text{c.g.}}$ splitting with the similar ψ'-η_c' splitting prediction is presented, and values for ψ'-η_c' have a range of order 20–50 MeV centered about 35 MeV. To range as high as the single experimental observation of 92 MeV for ψ'-η_c', such a poor fit to the seven levels is encountered that the model lacks any significant predictive power. Predictions for the $^3D_2$ and $^1D_2$ levels are also given.

PACS number(s): 11.10.Qr, 11.10.St, 12.40.Qq, 14.40.Jz

I. INTRODUCTION

The predictive power of a potential model with parameters is only in a limited sense given by the predictions with the best fit parameters. At the least one would like to give error bars to the prediction, which should arise by considering all "good" fits within a given range, their corresponding range of parameters, and the range of predictions given by this range of parameters. In actual fact the shape in parameter space of a surface of constant theoretical standard deviation calculated from experimental levels, ignoring experimental errors, is not a simple ovoid about the best fit, but a more complicated surface, which is bounded in three of the parameters, approaches an asymptotically constant shape in a fourth, and has a hyperbolic curvature in a pair of the parameters. In this paper we begin by showing such a contour shape in four variables of a six parameter fit. We then can make predictions which are weighted by the goodness of the fit. These are first shown for some levels separately. We then show the analogue of maximum likelihood plots where fixed standard deviation contours show the amount of correlations between predictions for two output level splittings. These are useful in using the information when one splitting is found to put further limits on an unknown splitting, and also to isolate the type of potential involved. In this paper we apply this to the charmonium spectrum and show the range of predictions for the $^1P_1$-$^3P_{\text{c.g.}}$ splitting, the ψ'-η_c' splitting, the $^3D_2$-$^3D_1(\psi')$ splitting, and also the $^1D_2$-$^3D_2$ splitting. The D_2 levels are supposed to have narrow widths due to having the wrong quantum numbers for decay into D-$\bar{D}$ states.

We use a relativistic bound state equation [1–6] which has a four component wave function, reduces in the nonrelativistic limit to the Schrodinger equation with Fermi-Breit spin-orbit, spin-spin, and tensor couplings, and reduces to the Dirac equation in the limit of a heavy fermion with a light fermion. The vector and scalar interactions are separated, with the gauge invariant vector interaction containing asymptotically free gluon exchange and the scalar interaction containing a linear potential plus a constant. In this paper we modify the previously considered interactions [1] by including two more parameters: a parameter c_0 in $\alpha_s(q^2) = (12\pi/27)/\ln(c_0 - q^2/\Lambda_R^2)$ and a constant V_0 in the linear scalar potential $V_S = \kappa r + V_0$. The bound-state equation was previously applied with good agreement to the charmonium spectra [1,2], to radiative transitions of charmonium and b quarkonium [7], to the 2γ and 2 gluon decays [8] of the η_c, and to f_B and the W-exchange contribution to the D_0 lifetime [9].

We demonstrate ways to visualize predictions in the space of the parameters of the potentials using isosurfaces of equally good overall fits. The values of a given prediction can be displayed by different values of gray scale or by different colors on these surfaces. We also demonstrate the minimum deviation or best fit method (the analogue of the maximum likelihood method) for finding the minimum standard deviation for a single value of a prediction or for a pair of predictions. The latter is shown in correlation plots. In a standard way of canceling spin-orbit and tensor contributions, we use the center of gravity (c.g.) of levels by weighting them by $(2J+1)$. We find that the predictions for the $^1P_1$-$^3P_{\text{c.g.}}$ splitting range from -6 MeV to $+4$ MeV for good fits to the spec-

tra (with $V_0 = 0.3$ GeV). We also find that the single experimental observation for the ψ'-η_c' splitting of 92 MeV can be accounted for only with such poor fits that any value from 12 MeV to 92 MeV is allowed, and in which the model then lacks any predictive power.

The errors or range of theoretical standard deviation of the fits for a given theoretical model is analogous to the statistical error associated with an experiment. The differences between different models which include different effects is then more analogous to the systematic error. Researchers often take for the range of predictions the less well-defined differences of predictions between models, while here we try to illustrate that each model also has its own intrinsic statistical range of uncertainty as well. Comparisons of the predictions between different models may well show overlaps of their statistical ranges of predictions. In this analysis, we use many parameters in order to simulate a whole range of models.

In Sec. II we describe the potential and the spectra we fit to. In Sec. III we describe the six parameters and show how we treat them to analyze all six of them together. In Sec. IV we show the multidimensional plots for good fit isosurfaces in the parameter space. Section V discusses limiting the mixing of C states in the formalism, which is not manifestly C conserving in the valence quark approximation. In Sec. VI we show the minimum deviation method for showing the range of predicted splittings and correlations between predictions. Section VII summarizes the use and value of these methods.

II. RELATIVISTIC INTERACTIONS, PARAMETERS, AND SPECTRA

We refer the reader to Ref. [1] for the formulation of the relativistic integral equation being used for charmonium. Here we only describe the modified interactions which include additional parameters. For the asymptotically free gluon exchange treated as a vector interaction coupling to γ_μ quark currents we use the form

$$V_V(q^2) = \tfrac{4}{3}4\pi\alpha_s(q^2)/q^2, \qquad (1)$$

$$\alpha_s(q^2) = (12\pi/27)/\ln(c_0 - q^2/\Lambda_R^2), \qquad (2)$$

where $q^2 = q_0^2 - \mathbf{q}^2$. The new parameter is c_0 which is kept greater than one so that the q^2 cuts are only in a physically correct region, and also since $c_0 = 1$ would result in the Richardson potential which has a Fourier transform which is linear in r. The linear potential must not occur solely in a vector interaction in a relativistic equation since it produces a Klein paradox with the lower Dirac components seeing a linearly falling potential. Studies of fits also show that the linear potential is best taken as scalar, as for example in Ref. [1]. In the plots, $\alpha_0 = \alpha_s(0)$, the value at $q^2 = 0$, will be shown instead of the parameter c_0, since the strength α_0 is more directly related to effects on the spectra, and since it is dependent only on c_0 and not on Λ_R:

$$\alpha_0 = \alpha_s(0) = (12\pi/27)/\ln(c_0). \qquad (3)$$

For the scalar interaction we use

$$V_S(r) = \kappa r + V_0, \qquad (4)$$

where V_0 represents the gluon field surrounding the quarks in addition to the linear part from the length of the string.

In order to get very accurate predictions we use only the seven well established levels of charmonium: namely, $J/\psi(3097)$, $\psi(3685)$, $\psi(3770)$, $\eta_c(2980)$, $\chi_{c0}(3415)$, $\chi_{c1}(3510)$, and $\chi_{c2}(3555)$. The η_c' has not been confirmed [10], and its location is far from our and other potential model calculations. The $\psi(4040)$ and $\psi(4160)$ are not unambiguously seen, and it is not easy to identify $\psi(4160)$ as the $2D$ state since it should have a small coupling to e^+e^- (see the minireview of the Particle Data Group [11], 1986). In any case, these two levels, along with the $\psi(4415)$, are expected to be heavily shifted and broadened by coupling with the D-$\bar{D}$ set of channels above threshold. Thus we constrain our search for good fits to the seven established levels listed above.

III. PARAMETERS AND THEIR RANGES

While we formally evaluate results for six parameters, to do it with finite computing time we take advantage of understanding the physical dependence on them. For the charm quark mass m_c we note that the spin-orbit and spin-spin splittings depend as m_c^{-2}, but the shift in m_c over the good fits is at most 300 MeV. The splittings thus vary slowly with m_c, but the overall levels shift together rapidly since the basic energy is $2m_c$. The mass m_c is therefore adjusted for each set of the other parameters to minimize the standard deviation of the calculated values of the seven levels from their experimental values. The final m_c is then an output function of the other parameters. This eliminates displaying the obvious variation in predictions with this parameter.

In varying the zero point of the linear potential, we take only a few values of V_0. Since the scalar V_0 adds to $2m_c$ to give the base meson mass for the spectra, a positive V_0 gives a lower m_c. To start each set of parameters then the η_c mass is calculated first from an initial m_c^0, and a δm_c^0 is found which is necessary to be added to give the η_c mass at its correct value. This is iterated again until no significant shift occurs. The effect is that the dynamical quark mass in the potential and splittings varies over the parameter ranges and enhances or decreases the splittings.

The theoretical standard deviation used for $N = 7$ levels is then formed from calculated levels E_c^i and experimental levels E_e^i (ignoring the small experimental errors) by

$$\sigma = \sqrt{\sum_{i=1}^{N}(E_c^i + 2\delta m_c - E_e^i)^2/(N-1)}. \qquad (5)$$

Each level is theoretically treated with equal weight. δm_c is chosen to minimize σ giving

$$0 = \sum_{i=1}^{N}(E_c^i + 2\delta m_c - E_e^i), \qquad (6)$$

$$\delta m_c = [1/(2N)] \sum_{i=1}^{N} (E_e^i - E_c^i). \qquad (7)$$

Equation (6) is equivalent to moving the center of mass of the calculated levels to that of the seven experimental levels. Using this δm_c in Eq. (5), the value of σ for each set of parameters is output. The final m_c is given by

$$m_c = m_c^0 + \delta m_c^0 + \delta m_c. \qquad (8)$$

Each level in the definition of σ is given equal theoretical weight as the minimum separation of the levels is at least 50 MeV and we are working with fits accurate to of order 10–15 MeV at most times.

The relativistic equation which is an extension of the Dirac equation requires a cutoff at high virtual three-momentum [1] p, and we take the strong form which has been needed for some calculations [9],

$$S(p) = 1/(1 + p^2/\Lambda_c^2)^2, \qquad (9)$$

making Λ_c the third parameter.

The parameter controlling the falloff of the vector coupling strength with q^2 is Λ_R^2. We observe in Eq. (2) that as Λ_R approaches infinity, the coupling strength approaches a constant, namely, α_0 in Eq. (3). Thus the surfaces of constant σ approach a shape which does not vary with Λ_R as it increases indefinitely. In practice, we find that beyond $\Lambda_R = 1$ GeV, there is little variation, and we use this as the upper limit for Λ_R in the calculations and figures.

In order to present minimum deviation plots (which are the analogue of maximum likelihood plots) and include contours up to $\sigma = 24$ MeV, we should include all parameters that yield such a σ or less. The shape of a fixed σ surface in the parameter space (see Fig. 1) is contained in all variables except Λ_R. Very large or small Λ_c will make the wave function at the origin and thus the spin-spin S wave splitting too large or small, respectively. So at a fixed σ the smallest and largest Λ_c parameters are contained. Very small Λ_R completely removes the attractive Coulombic-like potential and does not give good σ fits. The κ range is also bounded for a fixed σ. The lowest σ we get is about 8 MeV, and the "good fit" range of theoretical standard deviation about that is not quantifiable in terms of a confidence level, but as a matter of experience in making predictions and in the accuracy level needed for the specific predictions.

IV. ISOSURFACES OF STANDARD DEVIATION FOR THE CHARMONIUM LEVELS

Taking only certain values for V_0 we proceed to display the fixed σ surfaces in three-dimensional sections of the four variable space of Λ_R, κ, Λ_c, and α_0. With the above seven spectral levels and computing strategy, we found the best σ for $V_0 = 0.3$ GeV was about 9 MeV. Since most of the splittings are on the order of 100 MeV, in order to work to 20% accuracy we display the surfaces of $\sigma = 20$ MeV to make effects in the isosurfaces shape

clearer.

To begin, we demonstrate the relative constancy of the shape for Λ_R approaching 1 GeV. In Fig. 1(a) is plotted the surface for $\sigma = 20$ MeV, using the axes Λ_c, Λ_R, and α_0 for fixed $\kappa = 0.157$ GeV^2 and $V_0 = 0.3$ GeV. The ranges of the parameters for which all the calculations were made and plotted are $\Lambda_c = 1.5$–12.0 GeV, $\Lambda_R = 0.0$–1.0 GeV, $\alpha_0 = 0.1$–1.3, and $\kappa = 0.05$–0.30 GeV^2. In each parameter the calculations were carried out for 15 values uniformly spaced in the range. We note the effect in Eq. (2) that as $\Lambda_R \to \infty$, the strength α_s does not decrease with increasing $|q^2|$. Thus at large Λ_R the shape becomes
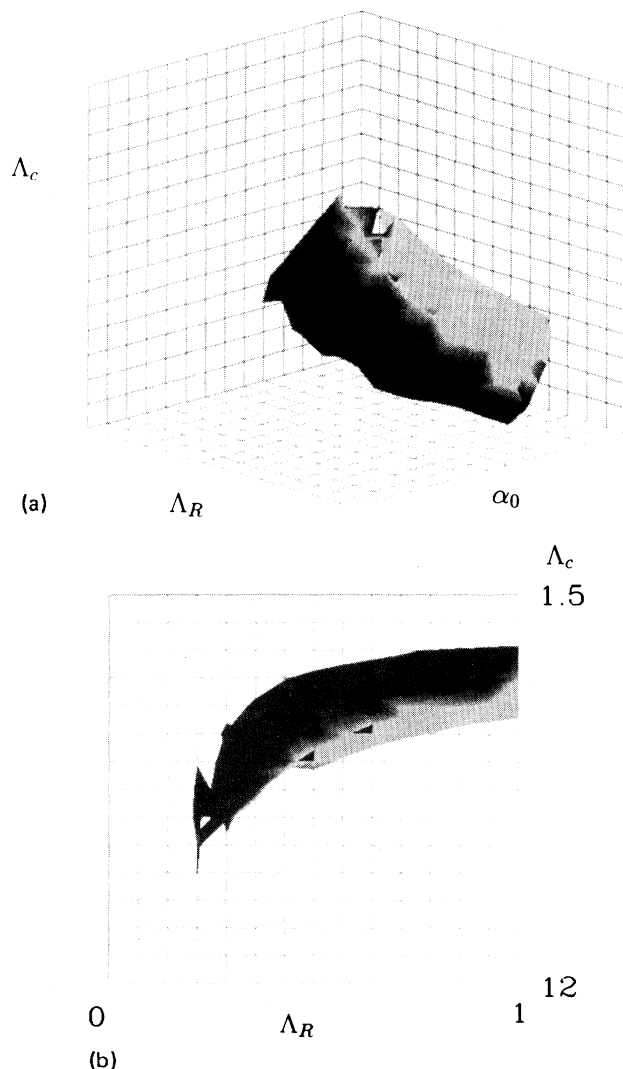

FIG. 1. (a) Surface of $\sigma = 20$ MeV for $V_0 = 0.3$ GeV and for fixed $\kappa = 0.14$ GeV^2 with Λ_c from 1.5 to 12.0 GeV, Λ_R from 0.0 to 1.0 GeV, and α_0 from 0.1 to 1.3. Predictions for the $^1P_1$-$^3P_{c.g.}$ splitting are displayed on the isosurface with gray for positive values and black for negative. (b) Same surface and shading but in Λ_R, κ, and Λ_c space for fixed $\alpha_0 = 0.5$, with κ from 0.05 to 0.30 GeV^2, and viewed down the κ axis into the Λ_R, Λ_c plane.

asymptotic or independent of Λ_R, as seen in Figs. 1(a) and 1(b). In this limit then, smaller α_0 is needed to give the same binding effect as Λ_R gets larger. Conversely, as Λ_R gets small, the logarithmic cutoff occurs rapidly, and larger α_0 is needed. In Fig. 1(b) is shown the $\sigma = 20$ MeV surface in the Λ_R, κ, and Λ_c space, viewed down the κ axis, for fixed $\alpha_0 = 0.5$. Again, the surface becomes asymptotic at large Λ_R. We also show in Figs. 1(a) and 1(b) the value of one of the predicted splittings by the grayness of the surface. In this case we show the $^1P_1$-$^3P_{\mathrm{c.g.}}$ splitting as gray where it is positive, and as black where it is negative. The positive range contains the experimental result [12] of Fermilab E760 of around 1 MeV for this splitting, and occurs for most Λ_R but only for $\alpha_0 \leq 0.7$, with larger α_0 needed for smaller κ.

The Λ_c cutoff acts in the integral over the virtual three-momentum p' of the momentum space integral equation [1] for the wave function $\psi(p)$ at momentum p. The

(a) $V_0 = 0.3$ GeV

$\sigma = 10, 15, 20$ MeV

$N_1(E_1)$

(b) $V_0 = 0$

$\sigma = 10, 15, 20$ MeV

$N_1(E_1)$

FIG. 2. Minimum deviation correlation plots of the fraction of the norm $N_1(E_1)$ of the $^3P_1$ amplitude (g_1) of the lower E_1 eigenvector versus the $^1P_1$-$^3P_{\mathrm{c.g.}}$ splitting for (a) $V_0 = 0.3$ GeV and (b) $V_0 = 0$.

$S(p, \Lambda_c)$ cutoff represents the physical effects of multi-quark or two-meson channels removing probability from the q-$\bar{q}$ channel in the integral equation. At small Λ_c, the effective strength is reduced by a lack of phase space, and is made up for in the good fits by an increase of the α_0 strength [Fig. 1(a)].

V. MIXING OF SPIN SINGLETS AND TRIPLETS IN THE QUARK OFF-SHELL RELATIVISTIC EQUATION

The single variable integral equation we use is obtained by taking matrix elements with the antiquark on mass shell and the quark off mass shell. This possesses some gauge invariance due to the on shell antiquark. This is computationally much simpler than the Bethe-Salpeter (BS) equation, where both antiquark and quark are off mass shell and both variables must be integrated over, and where all crossed gluon exchanges must be summed for gauge invariance. However, the lack of manifest charge conjugation (C) symmetry in the valence quark approximation will limit the predictions from the simpler quark off shell equation for mesons with C symmetry. Since the nonrelativistic reduction of the quark off shell equation gives the correct Fermi-Breit v^2/c^2 spin-spin, spin-orbit, and tensor interaction Hamiltonian, which conserves C, the solutions do not violate C in this limit.

The possibility for C violation appears in the angular-spin decomposition of the amplitudes in the integral equation where in the $L = J$ states the spin singlet amplitude (g_0) and triplet amplitudes (g_1) are mixed (see Ref. [1]), since relativistically $\mathbf{J}$ is a good quantum number, but $\mathbf{L}$ and $\mathbf{S}$ are not. This mixing occurs for the pairs ($^1P_1$, $^3P_1$) and ($^1D_2$, $^3D_2$) in this study. The mixing does not affect the ψ'-η_c' splitting or the fitting of the known levels, including having little effect on the $^3P_1$ level. We measure the mixing by the norms of the triplet (N_1) or singlet (N_0) amplitudes in a mixed state:

$$N_1 = \int g_1(p)^2 \Phi(p) dp, \qquad (10)$$

$$N_0 = \int g_0(p)^2 \Phi(p) dp, \qquad (11)$$

$$N_1 + N_0 \simeq 1, \qquad (12)$$

where $\Phi(p)$ is the phase space for the normalization and the sum is one when the small contribution of the lower Dirac components are included.

If we examine contours of equal standard deviation in plots of the fraction of the wave function in the triplet state $N_1(E_1)$ in the lowest of the mixed states of energy E_1 versus the $^1P_1$-$^3P_{\mathrm{c.g.}}$ splitting, Fig. 2(a) for $V_0 = 0.3$ GeV and 2(b) for $V_0 = 0$, we find for the $^3P_1$ waves that the triplet norm N_1 is 0.8–1.0, meaning that the mixing is only 0–20 %. From an example of a 2×2 Hermitian matrix with different diagonal elements and small mixing, we find that a small mixing in the wave function gives a correction to the level splitting equal to the same small fraction as the mixing in the normalization. Thus a 20% mixing only affects the predicted splitting by a mul-
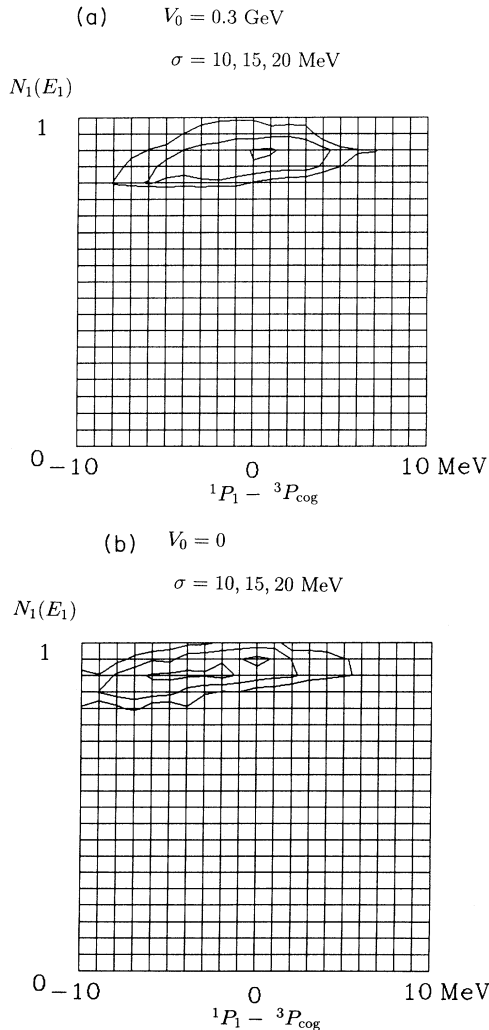
tiplicative factor of (1.0 ± 0.2) and we consider the results still as a good approximation, considering the simplicity of the quark off shell equation over the BS equation.

VI. RANGES AND CORRELATIONS OF PREDICTED SPLITTINGS

In describing the range of predictions for a given splitting, we consider separately each possible value of the splitting, and search over the entire parameter set for the minimum value of σ, Eq. (5), associated with that predicted value of the splitting. This could be plotted as a histogram over a given range of the splitting. For the cases of the mixed C states, we instead find σ contours in a plot of N_1, the triplet normalization, versus the splitting being considered (Figs. 2 and 4). In making predictions of two splittings simultaneously, and looking for their correlations, we search through the parameter range and find the minimum σ for each given choice of the two predicted splittings, and show the result with contours at fixed values of the minimum σ, with the predicted splittings as the axes (Figs. 3 and 5).

A. S and P wave splittings

We consider the levels or splittings being searched for in Fermilab E760 in proton-antiproton annihilation. The lowest σ range for the experimental $^1P_1$-$^3P_{\text{c.g.}}$ splitting $\simeq$ 1 MeV occur for $V_0 = 0.3$ GeV and are shown in Fig. 3(a). On the y axis is the splitting $\psi'(3686)$-η'_c from 0 to 100 MeV, and on the x axis is $^1P_1$-$^3P_{\text{c.g.}}$ from -10 to $+10$ MeV. The contours are at minimum σ of 10, 12.5, 15, 20, and 24 MeV. While the calculations over the parameter ranges of the potential were carried out by taking 15 uniformly spaced values in each range, the contours in this minimum deviation plot are smoothed over 20 bins in each of the axis variables, resulting in some roughness. The contours for $V_0 = 0$ are shown in Fig. 3(b) and the central contours are seen to be moved to about 3 MeV lower in the $^1P_1$-$^3P_{\text{c.g.}}$ splitting.

For $V_0 = 0.3$ GeV, Fig. 3(a), we see that predictions of $\psi' - \eta'_c$ peak around 30–40 MeV at the $\sigma = 10$ MeV contour, and range from 20 to 60 MeV at the $\sigma = 15$ MeV contour. The contour $\sigma = 24$ MeV is needed for $V_0 = 0$, Fig. 3(b), or for $V_0 = 0.3$ GeV, to reach the splitting of 92 MeV in the only observation [10,11] of the η'_c. At this $\sigma = 24$ MeV contour, the model lacks predictive power as the whole range from about 12 MeV to 95 MeV is included. Comparing Figs. 3(a) and 3(b) shows that the ψ'-η'_c splitting predictions are fairly independent of V_0, but the upper range is about 5 MeV higher for $V_0 = 0$.

The range of the $^1P_1$-$^3P_{\text{c.g.}}$ splitting for $V_0 = 0.3$ GeV in Fig. 3(a) is centered around zero at $\sigma = 10$ MeV and -5 to $+2$ MeV at $\sigma = 12.5$ MeV. For $V_0 = 0$ the $\sigma = 10$ MeV contour ranges from -7 MeV to about $+1$ MeV.

The new observation of the $^1P_1$ in Fermilab E760 [12] giving the $^1P_1$-$^3P_{\text{c.g.}}$ splitting at $+1$ MeV weighs somewhat in favor of $V_0 = 0.3$ GeV and indicates that these contours may be useful near the 10 MeV contours. These ranges may also be useful to experimenters to estimate what mass interval must be considered in which to eval-

uate the statistical significance of any peak found within this range. For $V_0 = 0.6$ GeV, the lowest σ contour is at 12.5 MeV and moves to too large a $^1P_1$-$^3P_{\text{c.g.}}$ of $+6$ MeV, indicating these higher V_0 values are not needed. For $V_0 = -0.6$ GeV, the best contour is at -4 MeV for the above splitting and the $+1$ MeV value has moved to the $\sigma = 12.5$ MeV contour, indicating that lower values of V_0 are not as useful.

The presence of a nonzero $^1P_1$-$^3P_{\text{c.g.}}$ splitting in our calculations is due to the fact that we do not use a pure $1/r$ Coulombic gluon potential, but have the extra asymptotic freedom logarithmic q^2 dependence built in [Eq. (2)], and also use a cutoff on momentum in the relativistic integral equation. The cutoff effectively limits $|q^2| = |(p - p')^2| < O(4\Lambda_c^2)$. Not allowing higher $|\mathbf{q}|$ is equivalent to an infinite repulsive barrier at an effective $r_c \approx 1/\Lambda_c$. The spin-spin splitting is proportional to $\nabla^2 V$ and vanishes for a $1/r$ potential in $L \neq 0$ wave functions. For potentials with $\nabla^2 V(r)$ always positive, in the generalized Fermi-Breit v^2/c^2 corrections, this split-
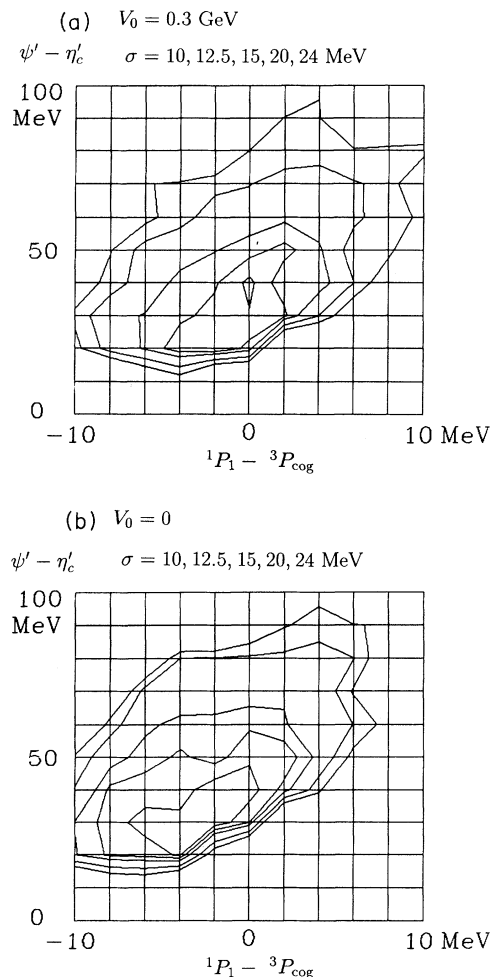

(a) $V_0 = 0.3$ GeV

$\psi' - \eta'_c$ $\sigma = 10, 12.5, 15, 20, 24$ MeV

(b) $V_0 = 0$

$\psi' - \eta'_c$ $\sigma = 10, 12.5, 15, 20, 24$ MeV

FIG. 3. Minimum deviation correlation plots between the ψ'-η'_c splitting and the $^1P_1$-$^3P_{\text{c.g.}}$ splitting, showing contours of $\sigma = 10$, 12.5, 15, 20, and 24 MeV, for (a) $V_0 = 0.3$ GeV, and (b) $V_0 = 0$.

ting will be negative with running coupling constants, but perturbative QCD allows both signs [13]. When the positive splitting values occur in this calculation they are at the larger Λ_c values where the relativistic effects are more important, and also at larger Λ_R where the q^2 falloff is lessened, putting more strength at higher $|q^2|$, as in the gray region in Fig. 1(b).

Both the ψ'-η_c' and the $^1P_1$-$^3P_{c.g.}$ are spin-spin splittings, and their magnitudes both depend on the shape of the short distance potential, and may be expected to show some correlation, as they do in Fig. 3(a) and 3(b). The lower limit on ψ'-η_c' is almost independent of the σ contour.

B. D wave splittings

The $^3D_2$ ($C = -$) and $^1D_2$ ($C = +$) are $J^P = 2^-$ and do not have the correct parity to decay to the D-$\bar{D}$

$J^P = 2^+$ states. Therefore their widths are suppressed, making them easier to find in a narrow energy bin search, and also enhancing their branching ratios to the J/ψ plus pion modes for Fermilab E760. The mixing between the $J^P = 2^-$ $S = 1$ and $S = 0$ wave functions in the quark off mass shell equation is illustrated in Fig. 4(a), where the contribution to the total norm of 1 from the $S = 1$ component with norm $N_1(E_1)$ of the lowest eigenvalue E_1 is shown versus the differences in calculated eigenvalues E_2-E_1. We see that there are two regions: one where $N_1(E_1)$ is close to 1, showing that the lowest E_1 state is the spin triplet $^3D_2$, and another where the $S = 1$ and $S = 0$ levels are too mixed to be identified with states of given C.

In studying the three-dimensional isosurfaces for $\sigma \leq$ 20 MeV, as in Fig. 1, on which we have instead displayed $N_1(E_1)$, we have found that as we stepped through α_0, that significant differences of $N_1(E_1)$ from 1 occurred
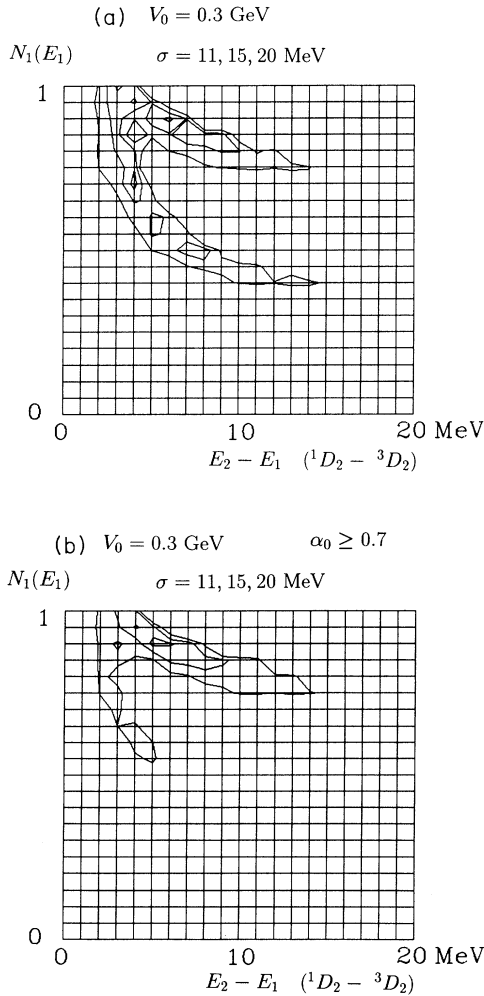

FIG. 4. Fraction of the norm $N_1(E_1)$ of the $^3D_2$ state amplitude g_1 in the lower E_1 eigenvector versus the level splitting E_2-E_1 for $V_0 = 0.3$ GeV, where in (a) all α_0 is used and in (b) only $\alpha_0 \geq 0.7$ is used, with contours at $\sigma = 11$, 15, and 20 MeV.
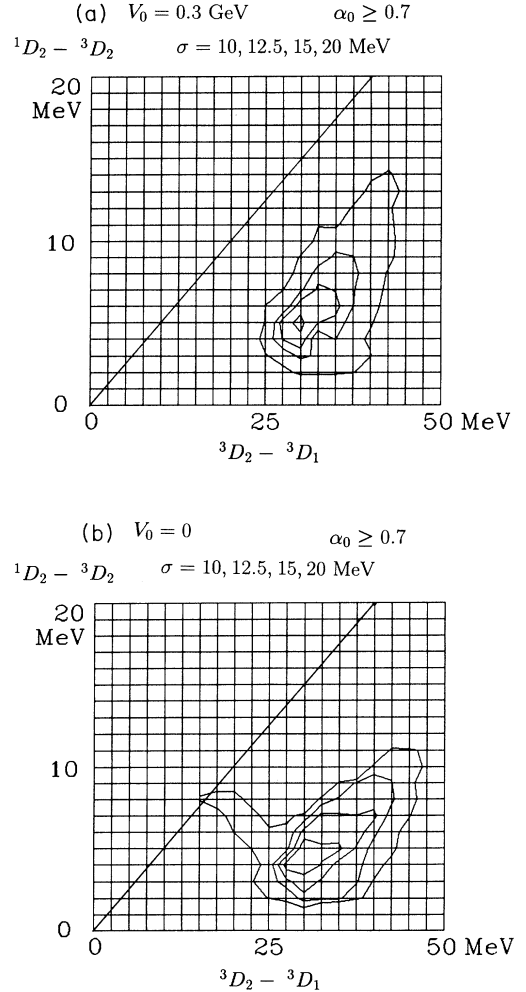
FIG. 5. Minimum deviation correlation plots between the $^1D_2$-$^3D_2$ splitting versus the $^3D_2$-$^3D_1(\psi'')$ splitting with $\alpha_0 \geq 0.7$ for (a) $V_0 = 0.3$ GeV and (b) $V_0 = 0$, showing contours of $\sigma = 10$, 12.5, 15, and 20 MeV. The diagonal line indicates the correlation if only spin-orbit splitting is involved.

when $\alpha_0 \leq 0.6$. Thus for $\alpha_0 \geq 0.7$ the lowest E_1 state is almost totally identified as the spin triplet $^3D_2$. In Fig. 4(b) we show the norm $N_1(E_1)$ versus $E_2 - E_1$ plot for $\alpha_0 \geq 0.7$ only, showing that the best fits with $\sigma = 11$ and 15 MeV have $N_1(E_1) \approx 1$ and the lowest E_1 state is the $^3D_2$. E_2 is then the $^1D_2$. The ranges with $N_1(E_1) \approx 1$ from Fig. 4(a) or 4(b) for E_2-E_1 or $^1D_2$-$^3D_2$ are our predictions for this splitting, namely, 3–6 MeV for $\sigma = 11$ MeV and 2–10 MeV for the $\sigma = 15$ MeV contours.

The splitting $^1D_2$-$^3D_2$ is shown versus the $^3D_2$-$^3D_1(\psi'')$ splitting for $\alpha_0 \geq 0.7$ with $V_0 = 0.3$ GeV in Fig. 5(a), and with $V_0 = 0$ in Fig. 5(b). The range of the $^3D_2$-$^3D_1$ splitting in Fig. 5(a) is seen to be 29–31 MeV for the $\sigma = 10$ MeV contour and 26–38 MeV for the $\sigma = 15$ MeV contour. For $V_0 = 0$ the ranges from Fig. 5(b) are 27–35 MeV for the $\sigma = 10$ MeV contour, and 26–43 MeV for the $\sigma = 15$ MeV contour. The $V_0 = 0$ ranges enclose the $V_0 = 0.3$ GeV ranges.

For the D wave splittings, we note that if the tensor force is small, especially for D waves as compared to P waves, then the splittings are given by spin-orbit splittings and are related. For the $^3D_2$-$^3D_1$ and $^1D_2$-$^3D_2$ splittings the differences in the values of $\mathbf{L} \cdot \mathbf{S}$ are 2 and 1, respectively. In Figs. 5(a) and 5(b), with x-axis $^3D_2$-$^3D_1$ and y-axis $^1D_2$-$^3D_2$ the spin-orbit correlation line running through zero is shown. Such a correlation is seen in the slopes of the contours, but not passing through zero. Thus a positive tensor force contribution of order 20 MeV is predicted in the $^3D_2$-$^3D_1$ splitting.

VII. CONCLUSIONS

In the isosurface of fixed σ in parameter space we have seen how changes in one parameter of the potential can be compensated by changes in another parameter. We have also seen by displaying predictions in gray scale across the isosurface whether a given prediction is "likely" by occurring over a large range of parameter, or whether it occurs only for a very small range of parameters, or at the extremes of the parameter range for good fits. We can further identify what features of the potential are important in each splitting. We also have seen how the shapes become asymptotic in one parameter and contained in others. Later, additional constraints can be added such as those from QCD calculations of the potential shape, and also radiative decay and annihilation rates. However, since our intent here was in making predictions for spectral levels, using them as the sole input and using their own deviation σ to evaluate the goodness of fit was the most consistent method.

We have also shown how to judge predictions and to find correlations in the minimum σ correlation plots. Ranges for predictions for η_c', $^3D_2$, $^1D_2$, and $^1P_1$ are then given. To name the most significant, we found that the $^1P_1$-$^3P_{\text{c.g.}}$ splitting can be positive as well as negative, and that the value of the ψ'-η_c' splitting ranges from 20 to 60 MeV, centered around 30–40 MeV.

ACKNOWLEDGMENTS

[1] M. Bander, D. Silverman, B. Klima, and U. Maor, Phys. Rev. D **29**, 2038 (1984).

[2] M. Bander, D. Silverman, B. Klima, and U. Maor, Phys. Lett. **13B**, 258 (1984).

[3] F. Gross, Phys. Rev. **186**, 1448 (1969).

[4] O. W. Greenberg, Phys. Rev. **139**, B1038 (1965); O. W. Greenberg and R. J. Genolio, *ibid.* **150**, 1070 (1966).

[5] K. Johnson, Phys. Rev. D **4**, 1101 (1972).

[6] G. P. Lepage, Phys. Rev. A **16**, 863 (1977).

[7] F. Daghighian and D. Silverman, Phys. Rev. D **36**, 3401

(1987).

[8] D. Silverman and H. Yao, Phys. Rev. D **36**, 3392 (1987).

[9] D. Silverman and H. Yao, Phys. Rev. D **38**, 214 (1988).

[10] C. Edwards, Phys. Rev. Lett. **48**, 70 (1982).

[11] Particle Data Group, M. Aguilar-Benitez *et al.*, Phys. Lett. **170B**, 1 (1986), p. 225.

[12] T. A. Armstrong *et al.*, Phys. Rev. Lett. **69**, 2337 (1992).

[13] D. B. Lichtenberg and R. Potting, Phys. Rev. D **46**, 2150 (1992); D. B. Lichtenberg, E. Predazzi, and R. Roncaglia, *ibid.* **45**, 3268 (1992).
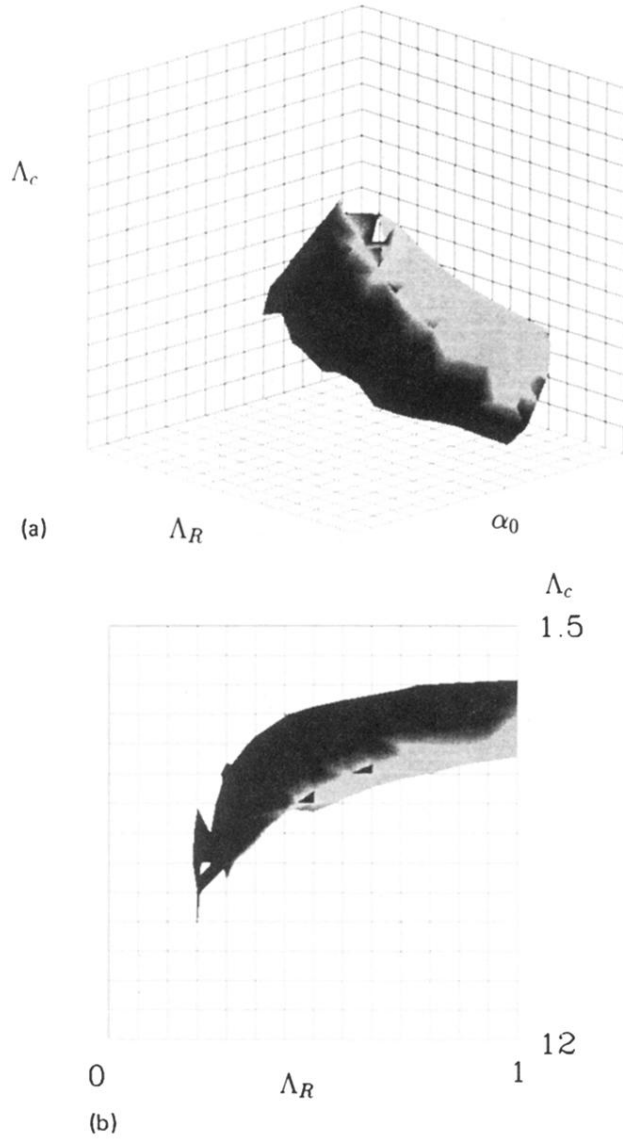
FIG. 1. (a) Surface of $\sigma = 20$ MeV for $V_0 = 0.3$ GeV and for fixed $\kappa = 0.14$ GeV^2 with Λ_c from 1.5 to 12.0 GeV, Λ_R from 0.0 to 1.0 GeV, and α_0 from 0.1 to 1.3. Predictions for the $^1P_1$-$^3P_{\rm c.g.}$ splitting are displayed on the isosurface with gray for positive values and black for negative. (b) Same surface and shading but in Λ_R, κ, and Λ_c space for fixed $\alpha_0 = 0.5$, with κ from 0.05 to 0.30 GeV^2, and viewed down the κ axis into the Λ_R, Λ_c plane.